On the role of dislocations in heavily strained YBa2Cu3O7-δ

Verwerft, M.; Dijken, D.K.; Hosson, J.Th.M. de; Steen, A.C. van der

Published in:
Ultramicroscopy

DOI:
10.1016/0304-3991(94)90153-8

Publication date:
1994

ELSEVIER

Ultramicroscopy 56 (1994) 135–143

ultramicroscopy

On the role of dislocations in heavily strained $YBa_2Cu_3O_{7-\delta}$

M. Verwerft [a], D.K. Dijken [a,b], J.Th.M. de Hosson [a], A.C. van der Steen [b]

[a] *Department of Applied Physics, Material Science Centre, University of Groningen, Nijenborgh 4, 9747 AG Groningen, The Netherlands*

[b] *TNO, Postbus 45, 2280 AA Rijswijk, The Netherlands*

Received in final form at the Editorial Office 10 August 1994

Abstract

Dense pellets of polycrystalline $YBa_2Cu_3O_{7-\delta}$ have been made by shock compaction. While $YBa_2Cu_3O_{7-\delta}$ is brittle at ambient conditions, the high pressure generated during the shock deformation is known to enhance its plasticity. Plastic deformation as well as fracture occurs when the shock wave passes through the initially loose powder, and multiple defects are expected to be generated. The paper reports on the interaction of dislocations with twin boundaries, and their role in the cleavage behaviour. The observations are performed on shock-loaded samples, compacted at E/M ratios ranging from 0.8 to 2.3. The microstructure of shock-compacted samples is compared to that of the initial, non-compacted powders. Apart from the well established $\langle 100\rangle\{100\}$ glide system, the role of the novel $[110](1\bar{1}0)$ and $[010](100)$ glide systems is studied. All glide systems are found to interact with the ferroelastic domains of the material, each in a different way.

1. Introduction

Dynamic compaction of high-T_c ceramic powders has been used as a technique to improve several properties of the material including:
(a) to obtain high density material and at the same time to improve the electrical contact between grains [1];
(b) to consolidate the initially loose powder and fabricate composite materials which incorporate stable, superconducting channels encapsulated in a metal matrix [2];
(c) to create defects in the superconducting powder grains, which could enhance the superconducting parameters such as critical field and current densities [3,4].

Because of the brittle nature of $YBa_2Cu_3O_{7-\delta}$, plastic deformation of this material is difficult. Its brittle character may, however, be suppressed either by performing deformation at elevated temperatures [5,6], at room temperature with the application of a confining hydrostatic pressure [7,8], or by performing shock-loading techniques [9,10]. The defect structure found after high-temperature deformation experiments may of course be different from the one found after room-temperature or shock-loading deformation. At elevated temperatures, diffusion-assisted climb of dislocations is likely to occur, whereas diffusion processes can be excluded in room-temperature and shock-loading deformation. Also the room-temperature deformation experiments performed under hydrostatic pressure do not necessarily yield the same microstructure as the present shock-loading experiments, since strain rates in shock-loading experiments differ by a factor of 10^9 from classical ("slow") deformation experiments.

The shock wave which propagates through the

SSDI 0304-3991(94)00116-2

initially loose powder is known to generate multiple defects. In a first approximation the shock loading of a powder sample is described as a large uniaxial strain imposed on an isotropic homogeneous sample [10]. The corresponding stress state may be decomposed in a hydrostatic and a deviatoric stress component. The hydrostatic stress component suppresses the brittle nature of $YBa_2Cu_3O_{7-\delta}$, and so plastic deformation with dislocation generation and motion is expected. In contrast to classical crystal deformation experiments which occur typically at strain rates of 10^{-5} to 10^{-1} s^{-1}, ballistic deformation experiments involve strain rates of 10^4 to 10^6 s^{-1}. These high strain rates yield completely different deformation mechanisms since defects cannot move the same way at high rates than they do at low rates [11]. The temperature may reach peak values of several hundred degrees centigrade during loading. These high temperatures, however, are only reached at the very boundaries of the grains. Moreover, cooling rates are very high (up to 10^9 °C s^{-1}). Any diffusion-assisted effects may thus safely be ignored.

2. Experimental procedure

The $YBa_2Cu_3O_{7-\delta}$ starting powder was prepared from commercially available "Rhone-Poulenc Superamic Y 200" powder, particle size 2–5 μm. This powder was heat-treated for 5 h at 950°C after which it was cooled to room temperature at a cooling rate of 2°C/min. The material was ground with a mortar and pestle and sifted to a particle size distribution of 6–36 μm, as determined with a "Malvern 2600 particle sizer". The oxygen content was determined with the wet chemical method [12] as 6.88 ± 0.01.

For the compaction of the $YBa_2Cu_3O_{7-\delta}$ powder, the widely applied cylindrical symmetric compacting configuration was used [13]. The $YBa_2Cu_3O_{7-\delta}$ powder is pressed to a 73.2% density in an aluminium tube, length 120 mm, inner diameter 16 mm (d_i), outer diameter 20 mm (d_o) and placed in the middle of a Teflon tube. The space between the Al tube and the Teflon tube is filled with a home-made powder explosive, containing 10% TNT, 84.2% NH_4NO_3 and 8.8% Al. Its detonation velocity is 3.76 km/s as measured with a set of nine ionisation pins. The specific mass of the explosive (ρ_{expl}) is 1085 kg/m^3, and the specific mass of the 73.2% dense $YBa_2Cu_3O_{7-\delta}$ powder (ρ_{powder}) is 4663 kg/m^3. The amount of explosives may be varied by using Teflon tubes of different inner diameter (D_i). If one puts $E = \frac{1}{4}\pi(D_i^2 - d_o^2)\rho_{expl}$ and $M = \frac{1}{4}\pi d_i^2 \rho_{powder}$ then the ratio of the mass density of the explosives to that of the material to be compacted, is expressed as the E/M ratio. Larger E/M ratios correspond to longer pulse duration and slightly higher peak pressures. The E/M values used in our experiments, are listed in Table 1. In the same table the average density of each of the samples is also listed.

Table 1
Experimental parameters and observed defects for the investigated samples

E/M	D (%)	Observed defects
Initial	–	Type A dislocations; twins
0.78	92.9	Above and type B dislocations
1.13	93.9	Above and $(1\bar{1}0)$, (103) cracks; $\frac{1}{6}(301)$ stacking faults
1.39	94.3	Above and type C dislocations
1.63	94.8	Above
1.95	94.6	Above
2.18	94.3	Above

Density (D) values are $\pm 0.7\%$. Notations concerning the labelling of the different types of dislocations are discussed in the text.

Samples for TEM analysis of the initial, non-compacted powder were made of a mixture of 70% $YBa_2Cu_3O_{7-\delta}$ powder and 30% epoxy. This mixture was put in a steel tube, with an inner diameter of 2.5 mm and an outer diameter of 3.0 mm. After hardening of the epoxy, thin slices were cut with a diamond saw. Both sides of the 3 mm disks are dimpled such as to obtain a centre thickness of 40 μm. The sample was finally ion-milled down to electron transparency with Ar^+ ions accelerated through 4 kV, a beam current of 0.5 mA and at an angle of 9°. For the compacted samples, thin slices were cut at the middle of the 120 mm tube. With an ultrasonic cutter 3 mm tube discs were cut near the Al tube wall, after

which the above TEM preparation procedure was followed.

Diffraction contrast experiments were carried out on a JEOL 2000CX electron microscope equipped with a side-entry goniometer and operated at 200 kV. The double-tilt sample holder allows tilting over $\pm 60°$ in one, and $\pm 45°$ in the other direction. High-resolution observations were performed with a JEOL 4000EX/II microscope equipped with a top-entry double-tilt stage allowing tilt angles of $\pm 20°$ in either direction. The latter observations were performed with a primary voltage of 400 kV.

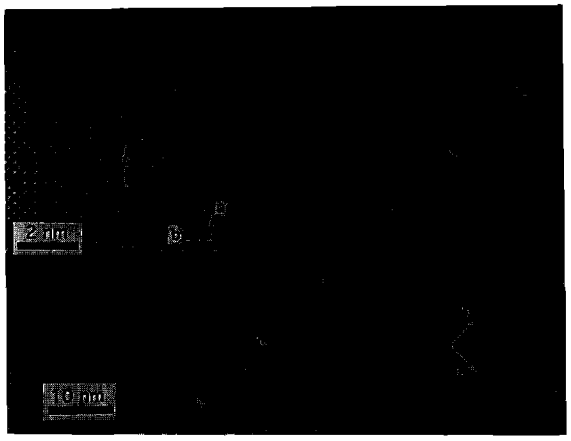

Fig. 1. High-resolution image in the [001] zone-axis orientation showing a pile-up of type C dislocations. The Burgers vector can be directly read from the atomic arrangement.

3. Observations and discussion

3.1. Dislocation classes and cleavage in $YBa_2Cu_3O_{7-\delta}$

All samples are orthorhombic and show twinning. Twinning in $YBa_2Cu_3O_{7-\delta}$ is related to the ferroelastic tetragonal-to-orthorhombic phase transition. In most cases, individual grains show twinning in only one direction. Twinning may of course occur on (110) as well as on $(1\bar{1}0)$ planes, but if a grain is twinned on only one set of planes, one is free to assign the (110) or the $(1\bar{1}0)$ planes to the domain walls. Throughout this analysis, we will adopt the convention that ferroelastic domain walls are indexed as (110) planes.

Three different types of dislocations are distinguished, which as for the sake of convenience will be named type A, B and C. Dislocations with [100] or [010] Burgers vectors gliding in the (001) planes have been observed frequently both in melt-textured samples and in room-temperature-deformed samples [5–8]. In neighbouring domains, the ***a*** and ***b*** axes are interchanged such that the Burgers vector of these dislocations are changed from [100] to [010] and vice versa. Since the contrast of such a dislocation does not change on passing from one variant to the other, we omitted to make a difference between the two types. In the remaining of the text, we will adopt the notation "⟨100⟩" or "type A" dislocations when referring to [100] or [010] dislocations without making a difference between both sets of dislocations. This notation tacitly refers to the parent phase tetragonal symmetry.

In the shock-deformed samples, pile-up arrays of [110] dislocations gliding in the planes perpendicular to the domain walls, i.e. the $(1\bar{1}0)$ planes, are observed. These dislocations will be called type B dislocations. The formation of pile-up arrays and cleavage along the $(1\bar{1}0)$ planes, and the interaction with the ferroelastic domain structure is discussed in Section 3.3.

Next to the well known type A dislocations and the novel type B dislocations, arrays of [010] dislocations gliding in the (100) planes are found. Their Burgers vector is identical to that of the type A dislocations, but the line of the type A dislocations is completely confined to the (001) plane, while the edge part of the latter type of dislocations runs parallel to the [001] direction. The latter type of defects thus forms a new class: type C dislocations. In Fig. 1, a high-resolution image of such a pile-up array is shown. The structure is imaged along the [001] zone-axis orientation. Edge parts of type C dislocations are then imaged end-on. In this orientation, one may directly determine the projected Burgers vectors, simply by drawing a circuit around the core of the dislocation. The inserted half-plane is easily observed in the enlarged inset if viewed under glancing angle. A complete discussion of the lat-

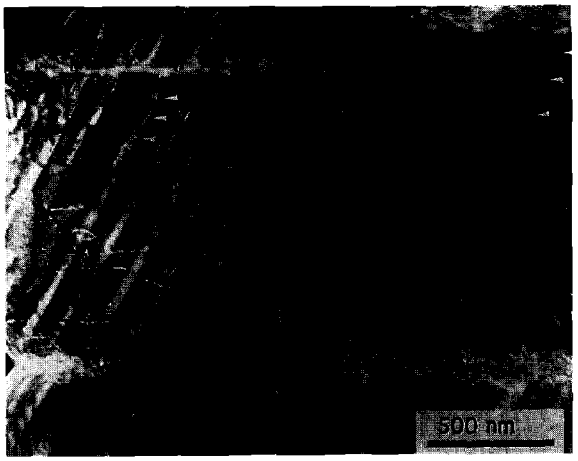

Fig. 2. (110) dark-field image tilted slightly away from the [1$\bar{1}$0] zone axis. The planar faults indicated by the large black arrows are cracks along the (103) plane. Dislocations observed in this picture are all of type A. They are mostly of the screw type, occasionally an edge part connecting two screw parts is observed (open arrows). Along the domain walls, segments of type A dislocations of mixed character running strictly parallel to the [1$\bar{1}$0] direction are found (small arrows, see also the inset in the right upper corner).

ter type of dislocations, together with their interaction with the ferroelastic domain structure, is presented elsewhere [9]. It should only be noted that cleavage along the (100) plane, i.e. the slip plane of this class of dislocations, does occur.

Cleavage along (103) planes (Fig. 2) is also observed. This cleavage process is, as far as we could see, not related to preceding pile-up formation. When regarding the $YBa_2Cu_3O_{7-\delta}$ structure as being built of perovskite blocks (as is often done irrespective of the wrong coordination of the constituting atoms), the (103) planes in $YBa_2Cu_3O_{7-\delta}$ are seen to correspond to the (101) planes in a perovskite.

3.2. Domain wall interaction

In as-grown material, the density of dislocations is below 10^6 mm^{-2}, and only type A dislocations are found. They form loops with more or less equal length of the edge and screw components. No interaction with the twins or the twin walls could be detected. The tetragonal-to-orthorhombic phase transition which occurs on cooling to room temperature apparently does not influence the dislocation arrangement.

The appearance of the type A dislocations changes drastically in the shocked material. In all compacted samples, the type A dislocations are predominantly of screw character. This is easily understood if one considers the fact that the mobility of edge dislocations is much higher than that of screws. During the deformation of the sample an initially round loop extends; the edge parts will thus first reach a grain boundary and disappear with the creation of a surface step. Our observations also confirm findings from slow deformation experiments [8], namely that the ferroelastic domain walls act as obstacles in the motion of the type A dislocations. When crossing a domain wall it is seen that they are pinned for some distance by the wall, and thus adopt mixed character, before continuing as a screw in the other domain (Fig. 2). A model for the interaction between type A dislocations and domain walls based on the core structure of the dislocations is presented elsewhere [9].

Core structures of these type A dislocations can be investigated through high-resolution observations. In Fig. 3, a region containing two

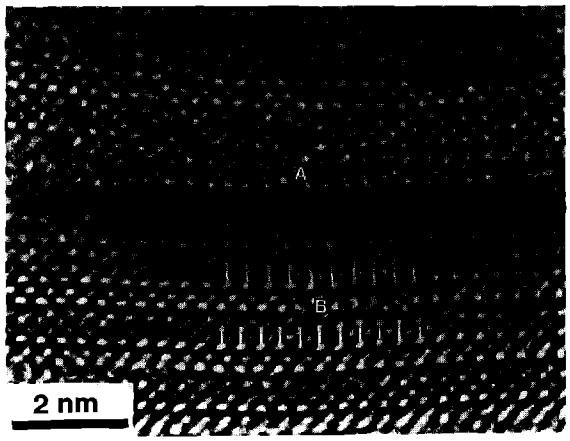

Fig. 3. High-resolution image along the [010] zone-axis orientation showing the core structure of type A dislocations. The core structure situated on a non-conservative stacking fault containing an extra CuO layer is indicated by the capital "A". Another dislocation core, but now in the otherwise perfect structure is indicated by the capital "B". In both cases, the dislocation core is situated on the CuO layer(s) in between two BaO layers.

remaining edge parts of type A dislocations is imaged in high resolution. The structure is imaged along the [100] orientation. The dislocations are then projected end-on, and one can determine their core structure from a comparison of experimental high-resolution images with computer-simulated ones. In particular this method allows one to determine the layers at which the cores of the type A dislocations are located. For both dislocations, their core is situated at the CuO layer in between the BaO layers. The dislocation indicated by a capital B runs through normal $YBa_2Cu_3O_{7-\delta}$ material. The dislocation indicated by capital A has its core situated on a stacking fault.

3.3. Pile-up and cleavage along (1$\bar{1}$0) planes

While type A dislocations are also observed in non-compacted samples, type B and type C dislo-

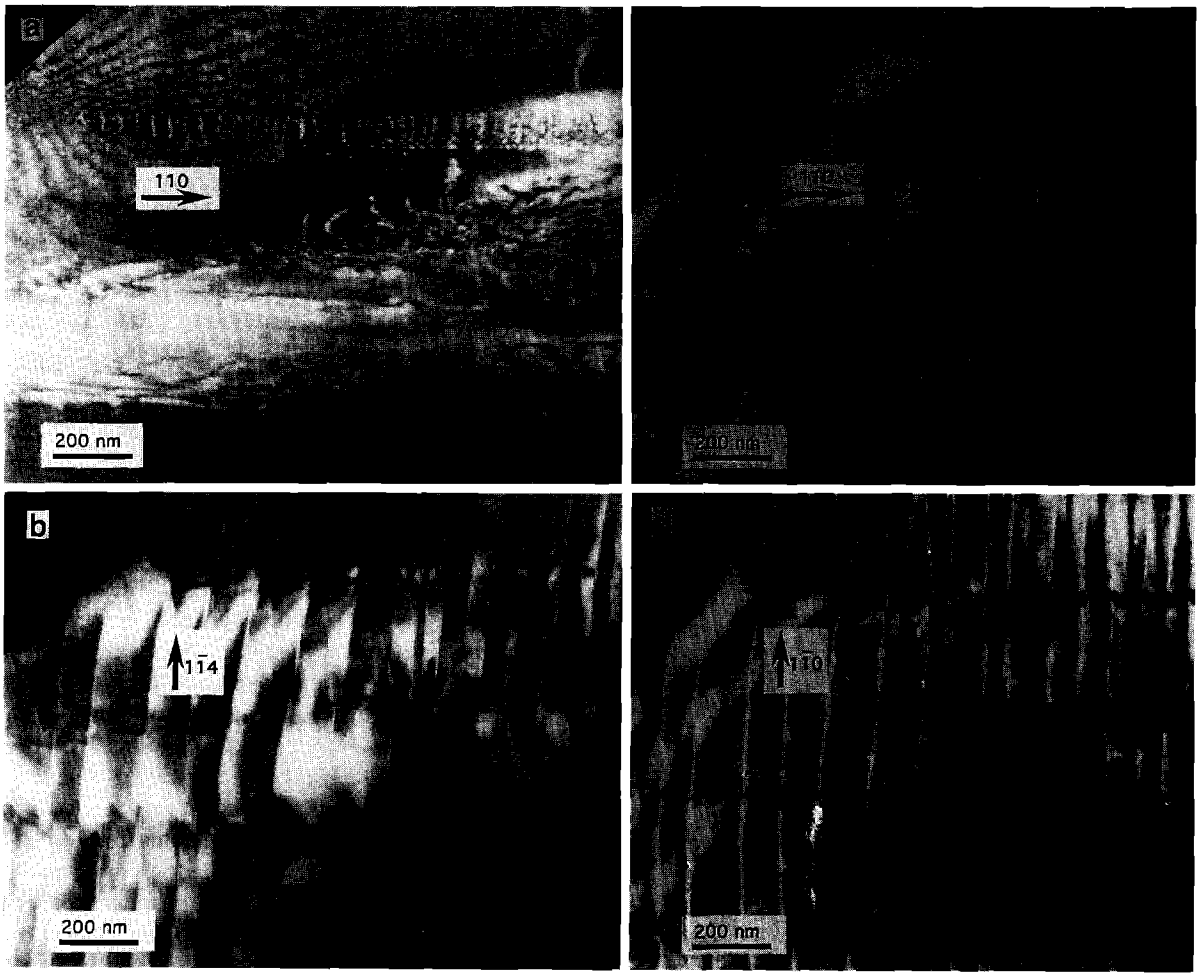

Fig. 4. (a) (110) dark-field image near the [$\bar{2}$21] zone-axis orientation. Three well defined pile-up arrays of [110] dislocations are observed and one less well defined cluster of dislocations of the same type. In two of these pile-up arrays, a Frank–Read source is clearly imaged. (b) (1$\bar{1}$4) dark-field image of the same area: all dislocations are out of contrast. (c) (110) dark-field image near the [001] zone-axis orientation. The dislocations in the pile-up arrays are now projected end-on or one on top of the other. (d) (1$\bar{1}$0) dark-field image in the same orientation as (c). The pile-up arrays are visible through residual contrast, but individual (1$\bar{1}$0) dislocations in the cluster are extinct.

cations are only found in deformed samples. We will first discuss the type B dislocations. Pile-up arrays perpendicular to the ferroelastic domain walls are observed in all the compacted samples. In the least shocked samples, only pile-up arrays are found, while in the more heavily shocked samples, both pile-up arrays and cleavage along the same $(1\bar{1}0)$ planes are observed. If the sample is oriented along the [001] zone axis, the pile-up arrays are projected edge-on (Figs. 4c and 4d), and they are imaged as straight lines perpendicular to the ferroelastic domain walls. When the sample is tilted away from the [001] zone axis about the [110] direction, the individual dislocations of the pile-up arrays can be imaged (Figs. 4a and 4b). From classical extinction rules, their Burgers vector is then determined as [110]. In Fig. 4a, Frank–Read sources for these dislocations are also seen. Near the source, the dislocations are widely spread, while further away, their spacing decreases and reaches a limiting value of 45 nm.

Reaction of two type A dislocations (one with a [100] and the other with a [010] Burgers vector) forming [110] dislocation segments is reported to occur occasionally [7]. The present observations show that these [110] segments can operate as Frank–Read sources. Conservative motion of the edge part of the [110] dislocations is only possible in the $(1\bar{1}0)$ planes. When the motion of the leading dislocation is impeded, a pile-up along the $(1\bar{1}0)$ plane is then formed. In the least shocked samples, several pile-up arrays of this type are observed. In the more heavily shocked material, cleavage cracks along the same $(1\bar{1}0)$ planes are observed rather than the pile-up arrays. Cleavage along slip planes occurs in hexagonal close-packed metals. Such a cleavage behaviour is assumed to be due to the tendency of dislocations to dissociate parallel to the glide plane [14]. When the resolved shear stress is high enough to force the dislocations in the glide plane closely together, the incipient cracks at the dislocation cores may coalesce and macroscopic cleavage along the slip band can occur. Cleavage along $(1\bar{1}0)$ planes can thus be understood in terms of dislocation creation and motion.

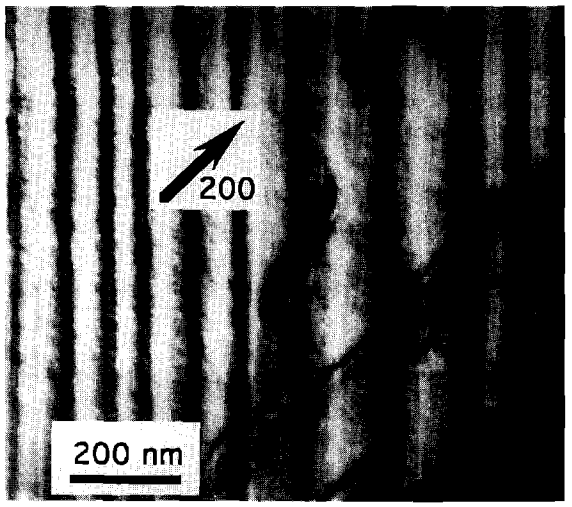

Fig. 6. (200) dark-field image of shocked material, showing type A dislocations. In the centre of the image, a type A dislocation is seen to run parallel to the [110] direction, without being confined to a domain wall. At other positions, type A dislocations are confined to a domain wall.

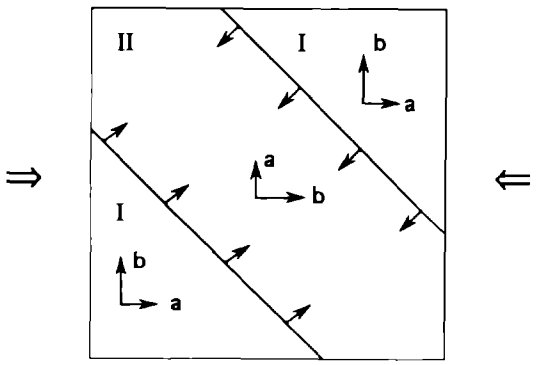

Fig. 5. Schematic representation of the usual set-up for the testing of ferroelastic poling of monocrystalline material. Uniaxial stress applied as indicated by the arrows evidently give rise to a tendency for domain II to shrink.

The model presented above does not provide an answer to the question why the pile-up arrays (and therefore also the cleavage) are always oriented along planes perpendicular to the ferroelastic domain walls. It will be shown below that this observation can only be understood if one assumes that the ferroelastic domain structure itself also plays a role in the deformation process. Domain switching with the application of external

pressure (ferroelastic poling, Fig. 5) is reported for monocrystalline $YBa_2Cu_3O_{7-\delta}$ [15]. Our experiments involve polycrystalline material, and since we do not know the initial distribution of the domains, it is not possible to decide by inspection of the domain structure alone, whether or not domain wall movement did occur or not. When inspecting the dislocation arrangement together with the domain structure, however, one does have a means to determine possible wall motion through the configuration of the type A dislocations. These type A dislocations, as discussed above, have a pronounced screw character in the deformed samples; only when traversing a domain wall, they sometimes are pinned for some distance and run along the [1$\bar{1}$0] direction. In Fig. 6, one observes a type A dislocation, which runs parallel to the [1$\bar{1}$0] direction (i.e. parallel to the domain walls), while it is not confined to a wall. Instead, it is running through the centre of a domain. This one and similar observations give evidence for the motion of domain walls during the deformation process. It is natural to assume that initially dislocations are pinned by a domain

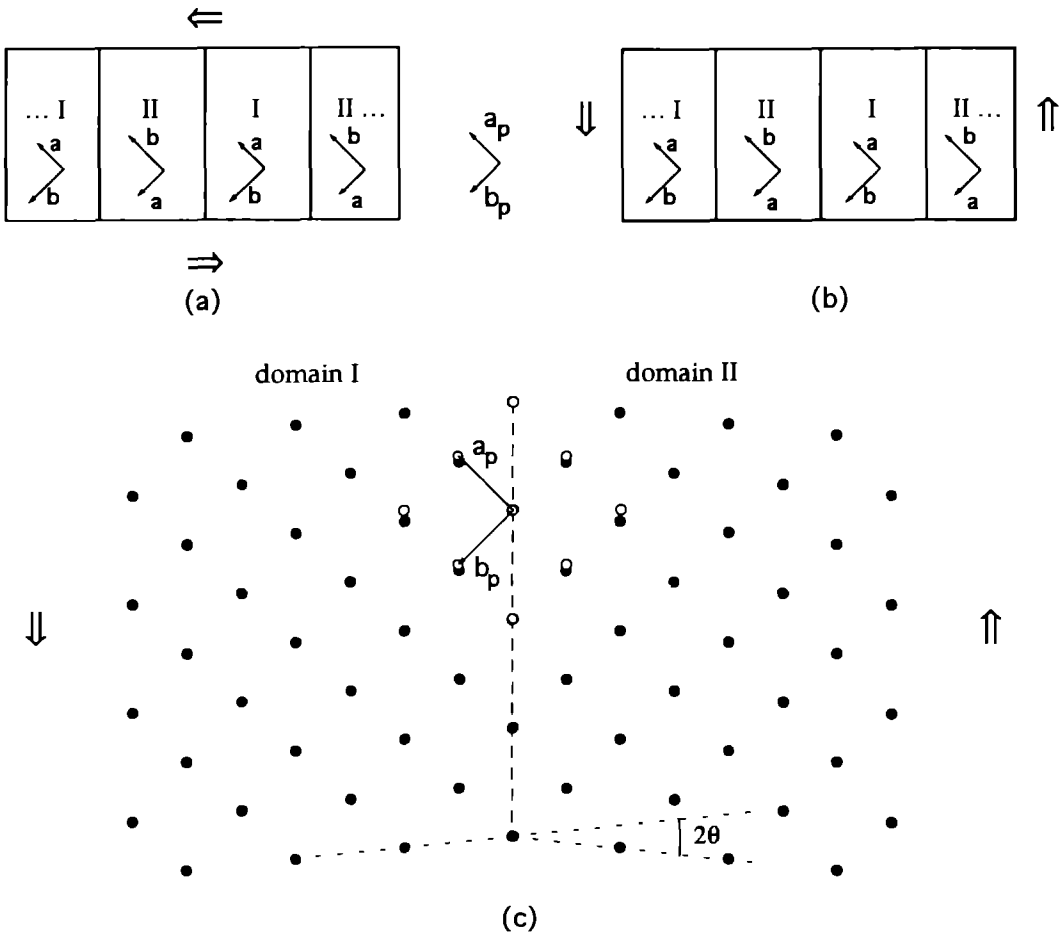

Fig. 7. (a) Schematic representation of simple shear (indicated by arrows) perpendicular to the domain walls; (b) simple shear parallel to the domain walls. Except for the domain wall configuration, this shear is identical to that of Fig. 7a. (c) Detailed schematic representation of the unit cell arrangement on either side of a domain wall, projected along the [001] direction.

wall and that in a second stage the domain wall itself moves.

We are now in a position to discuss the possible motion of domains under the action of shear stresses. $YBa_2Cu_3O_{7-\delta}$ belongs to the 4/mmm-mFmmm species of Aizu's classification of ferroelastic structures [16]. A property of ferroelastics is that their domains can be switched through an appropriate external stress. When testing ferroelastic domain switching, one usually applies a uniaxial compressive stress on a monocrystalline sample. It is evident that in the set-up depicted in Fig. 5, domain II will have a tendency to shrink. The fact that the crystal axes in the different domains are slightly rotated with respect to the parent phase axes is tacitly ignored. If, however, one also considers these rotations, it follows that also shear stresses act on the domain structure.

Pile-up arrays of type B dislocations as observed in Fig. 4 may be generated through the application of a simple shear stress perpendicular to the domain walls, as depicted schematically in Fig. 7a. The components of such a stress referred to the parent phase crystal axes read as:

$$\sigma_{11} = \sigma_{21} = -\sigma_{12} = -\sigma_{22}. \tag{1a}$$

The stress components of the situation depicted in Fig. 7b, referred to the same basis, read as:

$$\sigma_{11} = -\sigma_{21} = \sigma_{12} = -\sigma_{22}. \tag{1b}$$

One can then calculate whether or not the applied stress performs work when a ferroelastic domain is switched from one state to the other. The strain tensor describing the room temperature state of $YBa_2Cu_3O_{7-\delta}$ has two components different from zero: for one of both domains:

$$\varepsilon_{1,11} = -\varepsilon_{1,22} = -\delta, \quad \text{with } \delta = \frac{b_0 - a_0}{b_0 + a_0}. \tag{2}$$

The other domain has the opposite strain components. The strain tensor does not take into account that the ferroelastic domains are slightly rotated with respect to each other. When describing the deformation accompanying the ferroelastic domain switching, one should include also this orientation change (Fig. 7b).

The rotation angle with respect to the parent phase axes is obtained as:

$$\theta = \frac{\pi}{4} - \operatorname{arctg}\frac{a_0}{b_0} = \frac{\pi}{4} - \operatorname{arctg}\frac{\langle a\rangle - \Delta}{\langle a\rangle + \Delta} \approx \frac{\Delta}{\langle a\rangle} = \frac{b_0 - a_0}{b_0 + a_0} = \delta, \tag{3}$$

where the notation $\langle a\rangle = \frac{1}{2}(b_0 + a_0)$ is used for the high symmetry a parameter extrapolated to room temperature.

If one wants to include the body torques in the calculations, one is forced to work with the deformation tensor e_{ij}, rather than with its symmetric part only. For one of the two domains one has: $e_{1,11} = e_{1,21} = -\delta$ and $e_{1,12} = e_{1,22} = \delta$. For the other domain, one gets the opposite deformation $e_{II,ij} = -e_{1,ij}$. The difference in deformation between the two domains equals:

$$\Delta e_{11} = \Delta e_{21} = -2\delta, \quad \Delta e_{12} = \Delta e_{22} = 2\delta. \tag{4}$$

The work done by the external stress when one of the domains is switched to the other state is to the first order given by:

$$\Delta W = \Delta e_{ij}\,\sigma_{ij}. \tag{5}$$

If one combines (1a), (1b) and (4), it is seen that the stress depicted in Fig. 7a does not perform work when a ferroelastic domain is switched to the the other state, whereas the stress depicted in Fig. 7b does work when switching the ferroelastic domains.

This result allows us to interpret the observation that the pile-up arrays are always perpendicular to the ferroelastic domain walls. Indeed, if the stress acts parallel to the twin walls, the domain structure itself is altered. On the other hand, if the stress is applied perpendicular to the domain walls, the structure cannot respond by changing its domain arrangement, and dislocation creation, flow and finally cleavage occurs.

4. Conclusion

Cleavage along (100), $(1\bar{1}0)$ and (103) planes is observed in shock-deformed $YBa_2Cu_3O_{7-\delta}$. Two of these cleavage systems are related to the for-

mation of pile-up arrays of dislocations. The ferroelastic domain structure is also involved in the deformation behaviour. In particular, we have shown that if body torque is included in a domain structure model, shear stresses parallel to twin walls can give rise to domain wall displacement. This model explains why pile-up arrays of type B dislocations are always oriented perpendicular to the domain walls: a shear stress parallel to the twin walls results in ferroelastic domain rearrangements, and only a shear stress perpendicular to the domain walls gives rise to pile-up arrays and eventually cleavage.

References

[1] H. Yamamoto and A.B. Sawaoka, in: Shock Compression of Condensed Matter, Eds. S.C. Schmidt, J.N. Johnson and L.W. Davison (Elsevier, Amsterdam, 1990).
[2] L.E. Murr, A.W. Hare and N.G. Eror, Nature 329 (1987) 37.
[3] S.T. Weir, W.J. Nellis, M.J. Kramer, C.L. Seaman, E.A. Early and M.B. Maple, Appl. Phys. Lett. 56 (1990) 2042.
[4] K. Takashima, H. Tonda, M. Nishida, S. Hagino, M. Suzuki and T. Takeshita, in: Shock Compression of Condensed Matter, Eds. S.C. Schmidt, J.N. Johnson, L.W. Davison (Elsevier, Amsterdam, 1990).
[5] S. Nakahara, S. Jin, R.C. Sherwood and T.H. Tiefel, Appl. Phys. Lett. 54 (1989) 1926.
[6] T. Yoshida, K. Kuroda and H. Saka, Phil. Mag. A 62 (1990) 573.
[7] J. Rabier and M.F. Denanot, J. Less. Comm. Met. 164 (1990) 223.
[8] J. Rabier and M.F. Denanot, Phil. Mag. A 65 (1992) 427.
[9] M. Verwerft, D.K. Dijken, J.Th.M. De Hosson and A.C. Van Der Steen, Phys. Rev. B 50 (1994) 3271.
[10] M. Meyers, Scripta Met. 12 (1978) 21.
[11] L.E. Murr, Mater. Manufacturing Process. 6 (1991) 1.
[12] S. Bruckenstein and P.K. Wrona, Anal. Chim. Acta 237 (1990) 421.
[13] H.S. Yadav and K.R.K. Rao, Pramana J. Phys. 32 (1989) 47.
[14] E. Smith, in: Dislocations in Solids, Vol. 4, Ed. F.R.N. Nabarro (North-Holland, Amsterdam, 1983) pp. 418-419.
[15] H. Schmid, E. Burkhardt, B.N. Sun and J.-P. Rivera, Physica C 157 (1989) 555.
[16] K. Aizu, J. Phys. Soc. Jpn. 28 (1970) 706.